Chapter 3

Laser-Scribing Technology for Wafer-Scale Graphene Devices

He Tian, Mohammad Ali Mohammad, Wen-Tian Mi, Yi Yang and Tian-Ling Ren

Additional information is available at the end of the chapter

http://dx.doi.org/10.5772/64228

Abstract

Graphene has attracted a lot of attention due to its amazing properties. A huge number of novel devices, covering the electric, acoustic, photonic, magnetic and mechanical domains, can be developed with graphene. Its ultrahigh mobility can enable ultra-fast transistors or photodetectors. However, the natural zero bandgap of graphene, with insufficient on/off ratio, limits its practical applications. In this chapter, we introduce laser-scribing technology that enables wafer-scale production of graphene devices. Moreover, such laser-scribed graphene (LSG) is, infact, semi-reduced graphene oxide with a finite bandgap, which is suitable for practical applications. We show five kinds of representative LSG devices and their integration. These devices are a resistive memory, an earphone, a strain sensor, a pressure sensor and a light-emitting device. These LSG devices are high-performance, flexible and low cost, which demonstrates the practical nature of laser-scribed graphene-based materials. Finally, an outlook is presented regarding how laser scribing, a serial patterning method, may lead to similar developments in various other serial lithography techniques, such as ion beam lithography.

Keywords: graphene, graphene oxide, two-dimensional device, laser-scribing technology, laser reduction, nanoelectronics

1. Introduction

Graphene is a well-known two-dimensional material that has attracted wide attention due to its unique properties [1], which have not been observed in three-dimensional (bulk) materials. Graphene's mobility at room temperature can be as high as 200,000 $cm^2 V^{-1} s^{-1}$ [2], which

can be regarded as within the realm of ballistic transport and is much higher than the mobility of silicon. Moreover, graphene can absorb light in a wide range, even up to the far infrared [3], which is much broader than the capability of a conventional photodetector. Another powerful property is that its Young's modulus is 1 TPa [4], which makes it one of the strongest materials ever known. Graphene's thermal conductivity is also amazingly high at 5000 W/mK [5], which is also a record. Based on graphene's superior properties, a huge number of novel devices can be made using graphene, covering the electric, acoustic, photonic, magnetic and mechanical domains. However, graphene is not perfect. Its natural zero bandgap, with an insufficient on/off ratio, limits its practical applications. Especially, in logic circuits, the transistor needs to be turned off with a low current, which can reduce its power. This cannot be done in a graphene-based transistor, since the on/off ratio is only less than 10. Moreover, the current cannot be saturated under a high drain bias, which is also a drawback.

Figure 1. GO film obtained via the vacuum filtration method. (a) GO film on filter paper. (b) GO film on glass. (c) GO film on polyethylene terephthalate (PET). Reprinted by permission from Macmillan Publishers Ltd: Nature Nanotechnology (3:270), copyright (2008).[8].

A number of researchers tried to artificially introduce a bandgap in graphene. There are mainly three ways to do this. The first two ways consist of using a bilayer graphene and a graphene nanoribbon. The bandgap of bilayer graphene can only be opened around 30 meV, which is still not large enough. The graphene nanoribbon can provide sufficient on/off ratio, when the width of the nanoribbon is reduced down to 10 nm. However, the fabrication of graphene nanoribbon down to 10 nm is very challenging. Since these two methods cannot be scaled up, we refrain from discussing the details here. In this chapter, we mainly focus on the third method—using reduced graphene oxide (rGO). The bandgap of rGO can be tuned from 0~1.9 eV by controlling the quantity or level of reduction from graphene oxide (GO). Large scale graphene films have been prepared by chemical methods at low cost. A graphene oxide (GO) dispersion could be obtained by the Hummer's method [6], and the graphene oxide film can be prepared through various methods [7], that is spin-coating, spray-coating and vacuum filtration. Ultimately, the graphene film could be obtained by reduction. Some traditional methods include thermal and chemical reduction. Since there would be some oxygen functional groups remaining in the film after reduction, the width of the bandgap depends on how much oxygen will remain in the film. This can be tuned by controlling, for example, the reduction temperature. Large scale GO films can be prepared by a vacuum filtration method. This technique was firstly reported by Eda et al. (**Figure 1**), which revealed the application

http://dx.doi.org/10.5772/64228

potential of rGO in transparent electrodes and transistors [8]. The next step is how to control the shape of rGO.

Although large scale graphene films could be obtained by various methods, the laser-scribing procedure [9, 10] was developed to achieve a precise pattern of graphene, which had never been attempted before. The graphene pattern can be simply and cost-effectively obtained by a single-step laser scribing, even on flexible substrates.

The laser-scribing technology is a method in which a laser is used to convert the graphene oxide into reduced graphene oxide. With the use of the LightScribe DVD drive, specific patterns can be obtained. The laser (wavelength 788 nm, power 5 mW) in the LightScribe DVD drive can reduce the GO to rGO (**Figure 2a**). The laser can be controlled by a software, such as the Nero StartSmart software, and thus the input image can be printed onto the GO as rGO. An in-plane transistor array design is shown in **Figure 2b**, which could be revealed on the graphene film in ~25 min by laser scribing. The golden film in **Figure 2c** is graphene oxide and the black part is multilayer graphene. Complex graphics could also be converted into graphene patterns, such as the Tsinghua university logo, shown in **Figure 2d** and **e**. And a coloured picture could be converted into a greyscale graphene pattern (**Figure 2f** and **g**), in which the greyscale directly corresponds to the degree of reduction.

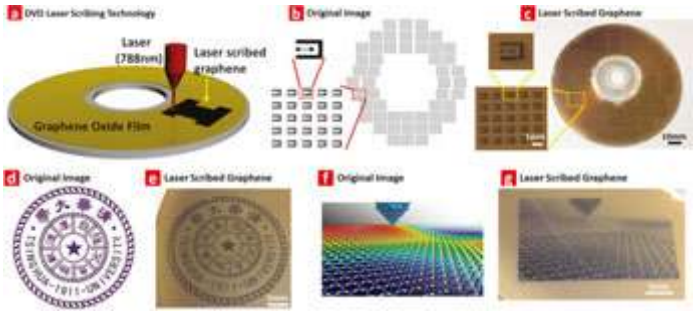

Figure 2. Demos of laser-scribed graphene. (a) Laser-scribing platform. (b) Layout for wafer-scale in-plane transistors. (c) Printed wafer-scale in-plane transistors. (d) An original image of the Tsinghua University logo. (e) The reproduced Tsinghua logo using LSG technology. (f) An original colourful image. (g) The printed LSG pattern in grey scale. Reprinted by permission from Macmillan Publishers Ltd: Scientific Reports (4:3598), copyright (2014) [16].

2. Characterization of laser-scribed graphene

In this section, we will demonstrate how to produce laser-scribed graphene(LSG) and discuss its characterization. The spot size of the laser, which is 20 μm in this work, determines the precision of the laser-scribed graphene. Post-exposure, it could be observed under an optical microscope that the laser-scribed graphene consists of long micro-ribbons (**Figure 3**). **Figure 3a** and **b** are the optical images of the laser-scribed graphene micro-ribbons under low magnification. Under visible-light irradiation, the GO is white and the rGO is black.

Increasing the magnification, a white line in the centre of the rGO micro-ribbon could be observed. Remarkably, different focus planes of GO and rGO, which are clearly shown in **Figure 3c** and **d**, suggest that the laser-scribed graphene micro-ribbon has a 3D structure. The total length of the rGO micro-ribbon can be very long (up to cm scale). If roll-to-roll technology is integrated with such laser-scribing technology, the length of rGO micro-ribbons can be even longer up to the meter scale. The most striking feature of the laser-scribing technology is that the rGO patterns can be obtained in a single step, which is time-efficient and low cost.

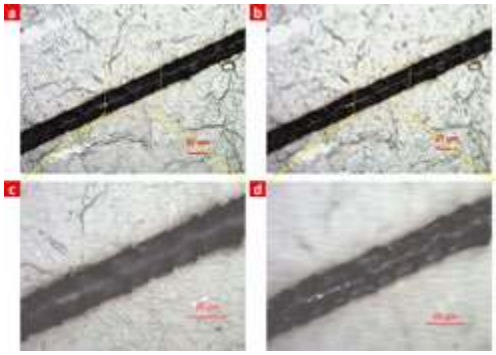

Figure 3. The optical image of a laser-scribed graphene micro-ribbon. (a) An optical image with focus on the GO surface. (b) The same optical image with focus on the rGO surface. (c) The zoomed-in image showing: (a) the GO surface and (d) the rGO surface, with z-direction profile.

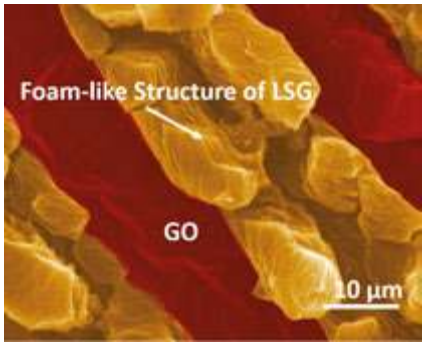

Figure 4. A false coloured SEM image of a laser-scribed graphene micro-ribbon. The red part shows the GO surface, and the yellow part shows the LSG foam-like structure. Reprinted from Ref. [14] (CC BY 4.0).

A falsely coloured SEM image (**Figure 4**) of laser-scribed graphene reveals the 3D structure more clearly. The red part in the image represents the GO, and the yellow part represents the

http://dx.doi.org/10.5772/64228

rGO. The contrast of light and shade in the image of the rGO ribbon indicates the valley in the centre and the elevation on the two sides, which resemble the foam-like structure.

The structural change of graphene before and after the laser scribing is shown in **Figure 5**. The thickness of the laser-scribed graphene is 10 μm, which is 10 times larger than that of the original GO film. It could be observed, in the magnified image, that the rGO is comprised of loosely stacked graphene layers and the GO film is made of dense layers. In the case of thermal reduction, a totally opposite behaviour is observed. The thickness of the graphene film decreases after thermal reduction, which results from the loss of the oxygen functional groups. However, the high-energy laser beam rapidly converts the oxygen functional groups into a gas containing oxygen, which finally leads to the loose structure of rGO and an increase of the total thickness.

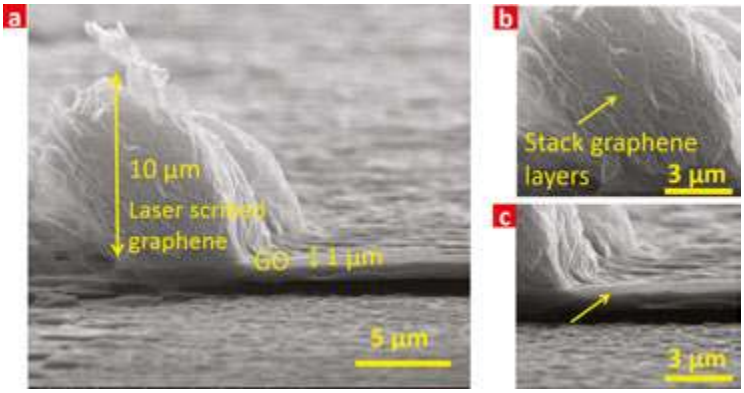

Figure 5. The lateral view of the laser-scribed graphene 3D structure. (a) A SEM profile showing the LSG and GO. (b) Zoomed-in image showing the loosely stacked graphene layers. (c) Zoomed-in image showing the dense GO film. Reprinted by permission from Macmillan Publishers Ltd: Scientific Reports (4:3598), copyright (2014) [16].

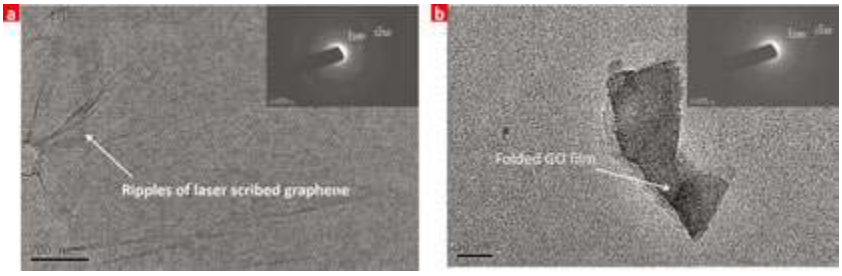

Figure 6. TEM images of (a) laser-scribed graphene and (b) GO (insets in both panels show the diffraction patterns from the atomic structure). Reprinted by permission from Macmillan Publishers Ltd: Scientific Reports (4:3598), copyright (2014) [16].

The diffraction pattern of the LSG (**Figure 6a**) confirms the hexagonal cellular lattice of graphene. On the contrary, the absence of a crystal lattice in the diffraction pattern of the stacked GO film (**Figure 6b**) indicates the broken C-C covalent bond, which results from the lattice defects bonding with oxygen functional groups.

Raman characterization is a quite efficient method to identify the properties of graphene. There are mainly three peaks present in graphene's Raman spectrum: the D-band (1350 cm^{-1}), G-band (1580 cm^{-1}) and 2D-band (2700 cm^{-1}). The D-band indicates the defects of the carbon lattice. If the D-band is strong, defects are present. The G-band position is sensitive to the doping level of graphene. If there is a right shift of the G-band, it means that the graphene is doped. The 2D-band/G-band ratio shows the layer number information. If the ratio is larger than 1, the film under inspection should be monolayer graphene. If it is around 1, then this is a strong indication of bilayer graphene. When the layer thickness number is larger than 3, the ratio is lower than 1. As shown in **Figure 7**, the change of the lattice structure could also be revealed in the Raman spectrum. The decrease of the D peak intensity suggests that part of the C–C bonds were repaired after the laser scribing. However, since there are still some defects left in the laser-scribed graphene, the D peak remains obvious. Besides, the left shift of the G peak indicates that the doping level of graphene decreased after the reduction, resulting from the removal of oxygen. And the appearance of the obvious 2D peak after the laser scribing indicates that the stacked multilayer graphene is generated after reduction.

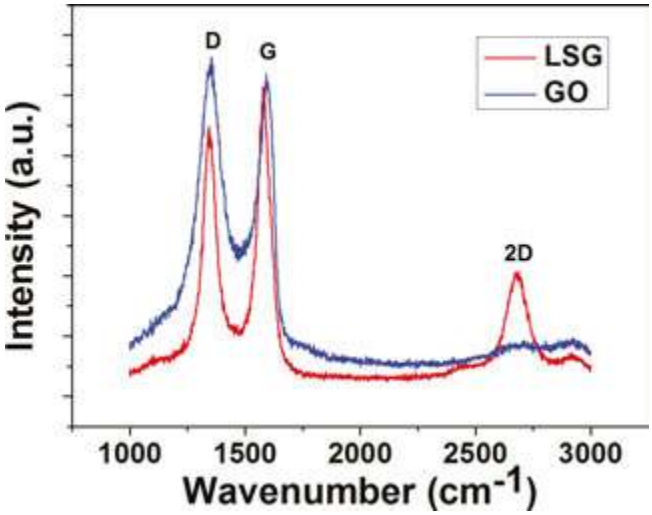

Figure 7. Raman spectra of GO and rGO.

X-ray photoelectron spectroscopy (XPS) is commonly used to identify the functional groups of various materials. Through the binding energy, the chemical formula and the electronic state of the elements can be revealed. The component of the laser-scribed graphene is shown in the XPS spectra (**Figure 8**). As shown in **Figure 8a**, the upper red spectrum is from the LSG and

http://dx.doi.org/10.5772/64228

the lower black spectrum is from the GO. Comparing the LSG spectrum with the initial GO film spectrum, the oxygen peak obviously decreases for LSG. This is a direct evidence that the laser can reduce the oxygen from GO. The C1s peaks are analysed carefully to identify the functional groups on the carbon lattice. After fitting the sub-peaks, the GO film contains the C–C, disorder, carbonyl and π–π bonds. By comparing the LSG, it shows that the peaks of the C–C sp^2 bond and π-π bond are enhanced after laser reduction.

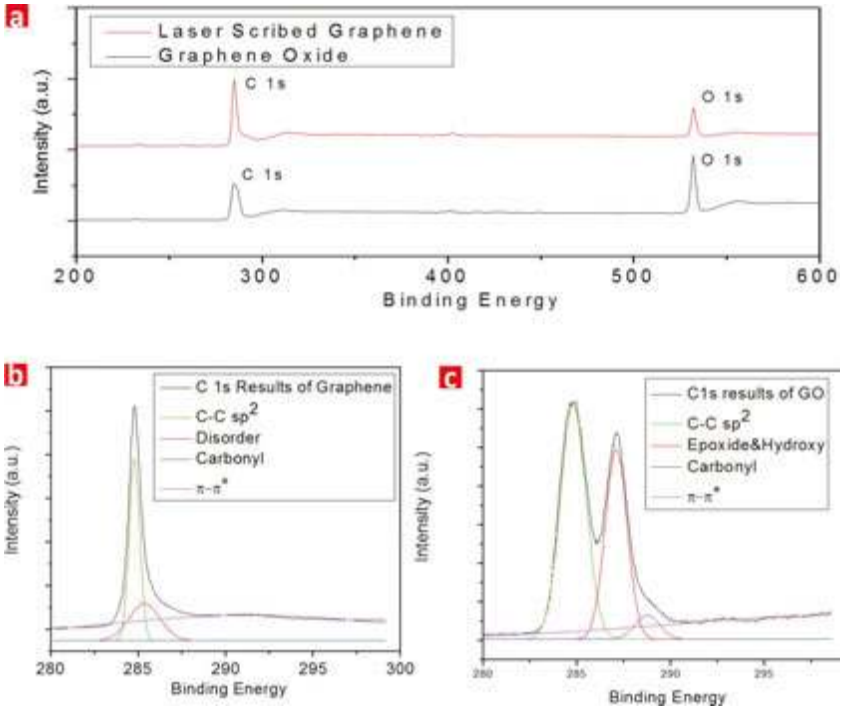

Figure 8. XPS spectra of GO and rGO. (a) The whole spectra of GO and rGO with the C_{1s} and O_{1s} peaks. (b) C1s peak of rGO. (c) C1s peak of GO.

3. LSG devices and their application

In this section, five different devices are presented, namely a memory device, an earphone, a strain sensor, a pressure sensor and a light emitter; all fabricated using laser-scribed graphene patterning technology. Each device will be presented in brief, while the readers are referred to the relevant citations to explore further details. Finally, multiple types of devices are patterned on the same surface in a single step, in close proximity, demonstrating the tremendously useful integration potential of this technique.

3.1. Graphene resistive random access memory

Using laser-scribing technology, a flexible graphene resistive random access memory or resistive memory (RRAM) [11] with a Fin-FET-like structure (**Figure 9a**) can be developed, which has great potential to increase the robustness of the device.

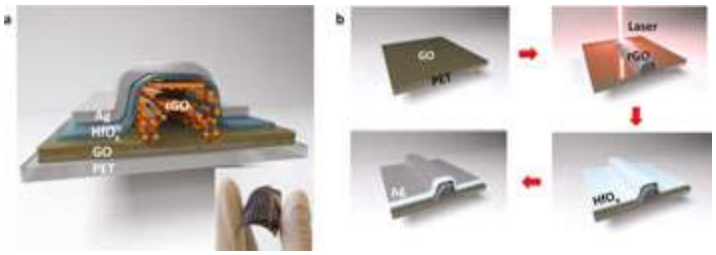

Figure 9. Flexible graphene RRAM device structure and fabrication process. (a) Device structure. (b) Fabrication process. Reprinted with permission from Nano Letters 14:3214. Copyright (2014) American Chemical Society [11].

As shown in **Figure 9b**, the GO dispersion was first spin-coated on the flexible polyethylene terephthalate (PET) substrates, following which the GO could be converted into rGO at specific locations. Then, the HfO_x and the silver top electrodes were deposited and patterned consecutively. For further details of the fabrication process and the testing method, please refer to Ref. [11].

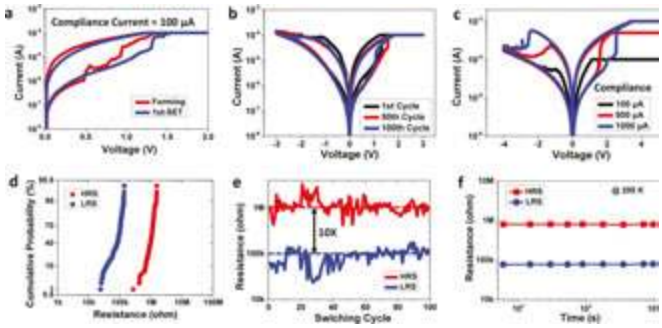

Figure 10. Measurement results of the flexible graphene RRAM. (a) Forming process. (b) Switching performance in the first, 50th and 100th cycles. (c) Switching curves under different compliance currents. (d) High- and low-resistance-state distribution. (e) High- and low-resistance-state under different cycle numbers. (f) Retention testing up to 10^4 s for both high- and low-resistance-state. Reprinted with permission from Nano Letters 14:3214. Copyright (2014) American Chemical Society [11].

The excellent performance of the flexible graphene RRAM is clearly shown in **Figure 10**, including the forming-free feature (**Figure 10a**), repeatability (**Figure 10b**), multi-valued feature (**Figure 10c**), uniformity (**Figure 10d**), feasible memory window (**Figure 10e**) and stability (**Figure 10f**).

http://dx.doi.org/10.5772/64228

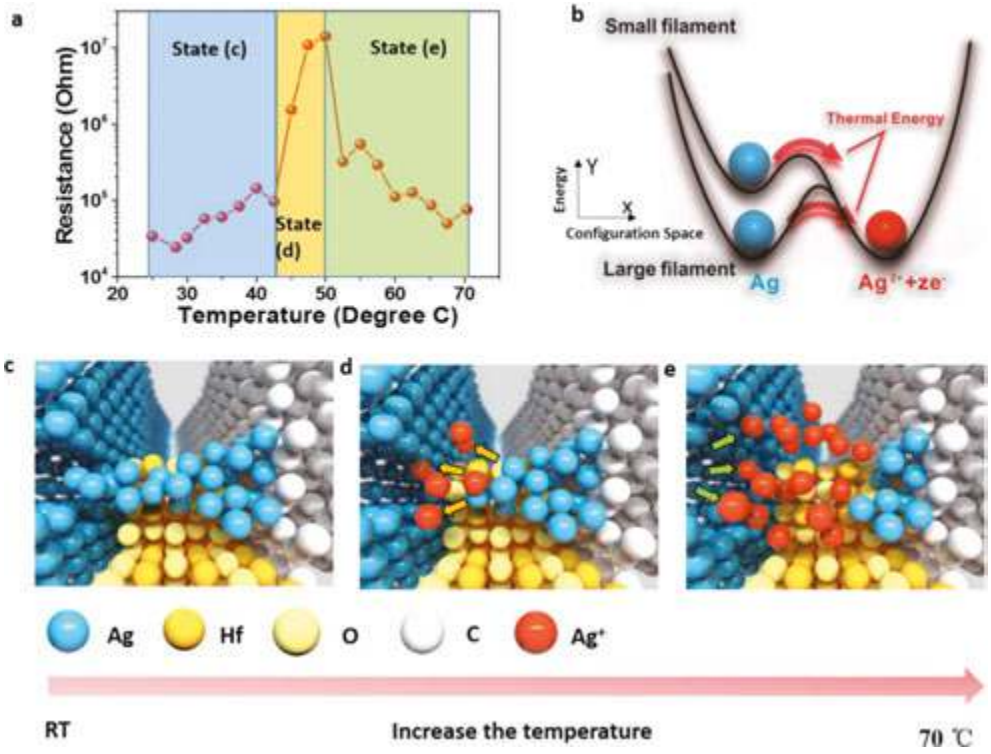

Figure 11. The working principle of the LSG RRAM. (a) The on-resistance *versus* the temperature. (b) The energy diagram for the filament formation. (c,d,e) The dynamic process in the filament region under increasing temperatures. Reprinted with permission from Nano Letters 14:3214. Copyright (2014) American Chemical Society [11].

The working principle of the graphene RRAM could be revealed by the temperature characteristics analysis (**Figure 11**). When the temperature is raised, the increase of the resistance indicates that the conductive filaments are made of silver. As the temperature is continually raised, some silver filaments transform into silver ions, leading to the increase of the resistance. As the silver ions are also conductive, if they increase, the resistance falls again.

This working principle may be confirmed by electrical measurements. The threshold voltage is only 0.5 V when the top electrode is made of silver. But for the device with Pt top electrodes, the threshold voltage is 2 V, which suggests that the soft breakdown voltage of the HfO_x is 2 V. Therefore, it is obvious that the HfO_x could not be broken down under 0.5 V, to form the oxygen filament, which confirms the claim that the filament is made of silver.

3.2. Graphene earphone

Flexible graphene earphones[12] can also be fabricated based on the laser-scribing technology. Compared with traditional earphones, the graphene earphone has the characteristics of flexibility and ultra-low thickness.

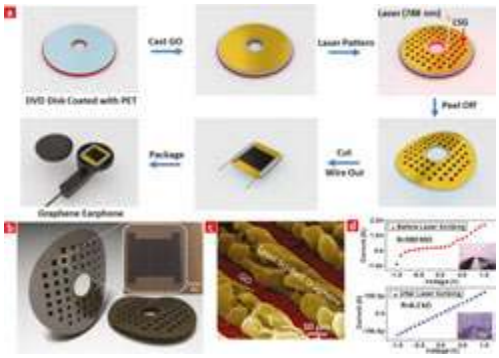

Figure 12. Graphene earphone. (a) Fabrication process of the graphene earphone using laser-scribing technology. (b) Wafer-scale graphene earphone after the laser scribing (inset showing the image of a single device). (c) SEM image showing the LSG profile. (d) I–V electrical properties before and after the laser scribing. Reprinted with permission from ACS Nano 8:5883. Copyright (2014) American Chemical Society [12].

Using the laser-scribing technology, the graphene sound source array could be fabricated on a PET substrate (**Figure 12a** and **b**). The I–V curve indicates the good conductivity of the graphene device. The sound source was wired out and packaged into a commercial earphone case (**Figure 13**). Further details about the fabrication and testing can be found in Ref. [12].

Figure 13. Packaged graphene earphone. (a) Graphene earphone in hand. (b) Graphene earphone after packaging. (c) The 3D assembled structure of the graphene earphone. (d) A pair of graphene earphones. Reprinted with permission from ACS Nano 8:5883. Copyright (2014) American Chemical Society [12].

The acoustic properties of the graphene earphone are tested on the measurement system, as shown in **Figure 14a**. The test results indicate that the sound pressure level of the frequency spectrum is flatter than that of commercial earphones, especially in the ultrasonic band. Moreover, the frequency spectrum of the graphene earphone covers not only the audible band (from 20 Hz to 20 kHz for human being) but also the ultrasonic band (from 20 to 50 kHz), which is the audibility zone for some animals. This implies that the graphene earphone could be a

http://dx.doi.org/10.5772/64228

useful tool for interspecies communication, which is also demonstrated in **Figure 15**. The 35 kHz acoustic signal is conveyed to a dog via graphene earphones, and with the aid of some prior training, the dog stood up as soon as the signal was delivered (**Figure 15**).

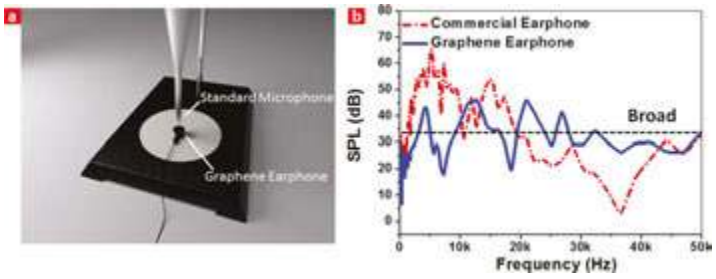

Figure 14. Performance testing of the graphene earphone. (a) Acoustic test platform for the graphene earphone. (b) Acoustic spectrum of the graphene earphone compared with a commercial one. Reprinted with permission from ACS Nano 8:5883. Copyright (2014) American Chemical Society [12].

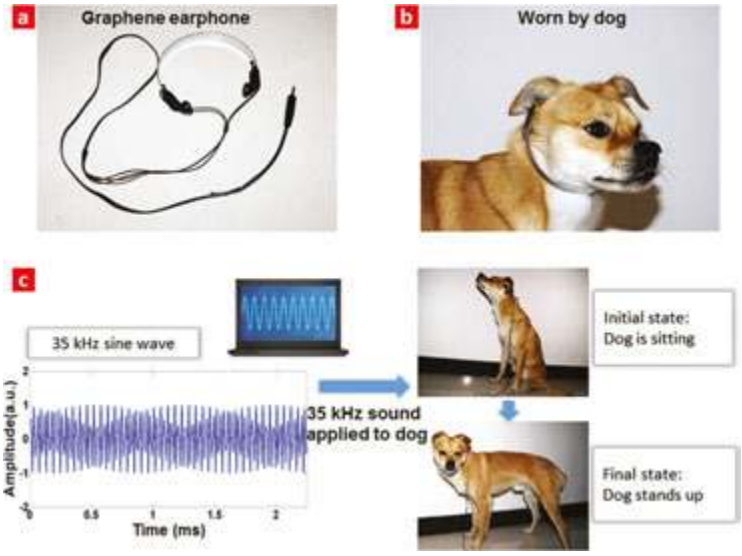

Figure 15. The graphene earphone as a tool for interspecies communication. (a) A pair of graphene earphones. (b) A dog wearing a graphene earphone. (c) Sound waves at 35 kHz applied to the dog signals it to stand up. Reprinted with permission from ACS Nano 8:5883. Copyright (2014) American Chemical Society [12].

3.3. Graphene strain sensor

Strain sensors are widely used in various application areas, but most of them are based on rigid substrates, which limit the sensitivity of the sensor. Using laser-scribing technology, a

flexible graphene strain sensor [13] is achieved with greatly enhanced sensitivity. The sensitivity (GR) can be expressed by the following equation:

$$GF = (\Delta R / R) / \varepsilon \tag{1}$$

Where $\Delta R/R$ is the relative resistance change, and ε is the applied strain.

The pattern of the graphene strain sensor array could be fabricated on the GO film via laser-scribing technology on a flexible PET substrate with low cost and high speed (**Figure 16**). The laser-scribed graphene is made of a loose stack of graphene layers, which could greatly enhance the sensitivity of the graphene strain sensor.

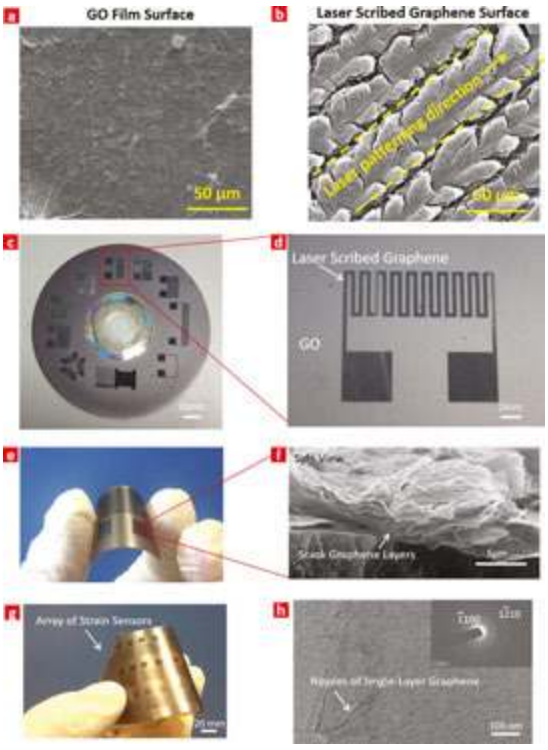

Figure 16. Graphene strain sensor. (a) SEM image of the GO surface. (b) LSG surface showing the direction of the laser movement. (c) Wafer-scale strain sensor with different shapes. (d) One strain sensor image. (e) Strain sensor showing good flexibility. (f) Cross-section image of the LSG film. (g) Array of graphene strain sensors. (h) TEM image showing the single-layer graphene. Reprinted from Ref. [13] with permission of The Royal Society of Chemistry.

The test results of the graphene strain sensor are shown in **Figure 17**. The sheet resistance was recorded while stretching the sensor. The sensitivity calculated from the data is 9.49, and **Figure 17f** indicates the rapid response of the graphene strain sensor. Commercial strain

http://dx.doi.org/10.5772/64228

sensors based on metal have a gauge factor of 2~5. Our LSG strain sensor has a much higher sensitivity as compared to commercially available strain sensors, which enables it to have a wide variety of applications. The working principle can be explained as follows: LSG contains a lot of graphene sheets. The conductivity of LSG depends on the overlapping area of the graphene sheets. When the LSG is stretched, the overlapping area of graphene sheets decreases, which increases the resistance. Therefore, by measuring the resistance change, one can know the strain applied to the LSG.

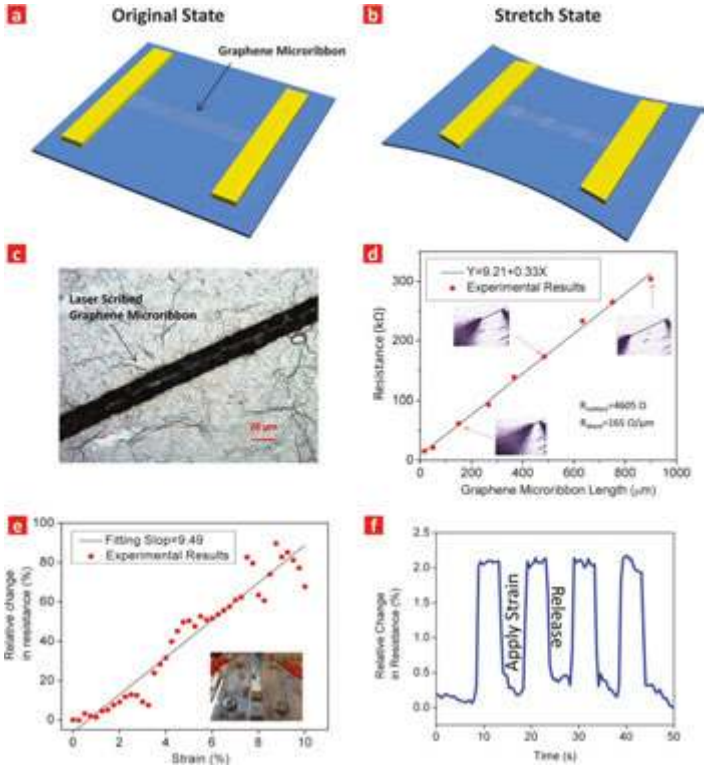

Figure 17. Test results of the graphene strain sensor. (a) Graphene micro-ribbon sensor in its original state. (b) Graphene micro-ribbon sensor in its stretched state. (c) Optical image of the graphene micro-ribbon. (d) Resistance *versus* length. (e) Relative resistance change *versus* strain. (f) Dynamic response to instantaneous force. Reproduced from Ref. [13] with permission of The Royal Society of Chemistry.

3.4. Graphene pressure sensor

Graphene pressure sensors can also be obtained by laser-scribing technology [14]. Conventional pressure sensors only have good sensitivity at pressure ranges lower than 5 Pa. However, the sensitivity will obviously decrease when the pressure is larger than 5 Pa. It is thus necessary to develop pressure sensors with high sensitivity over a wide range of pressures.

As shown in **Figure 18**, the core device structure is a stacking over of the two LSG layers with the patterns oriented perpendicularly to one another. The upper layer is oriented in the *y*-direction, and the lower layer is oriented in the *x*-direction. The profile of the LSG has a "V" shape with a height of 10.7 μm and a width of 19.8 μm. The fabrication process is illustrated in **Figure 19**, and the complete process details are provided in Ref. [14].

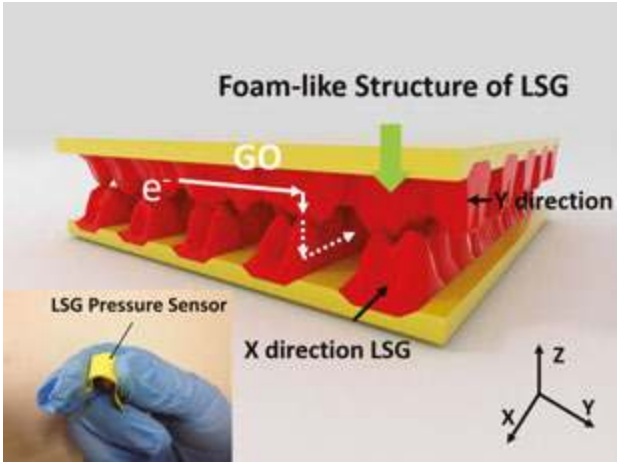

Figure 18. Device structure of LSG pressure sensor (the inset shows the real device in hand). Reprinted from Ref. [14] (CC BY 4.0).

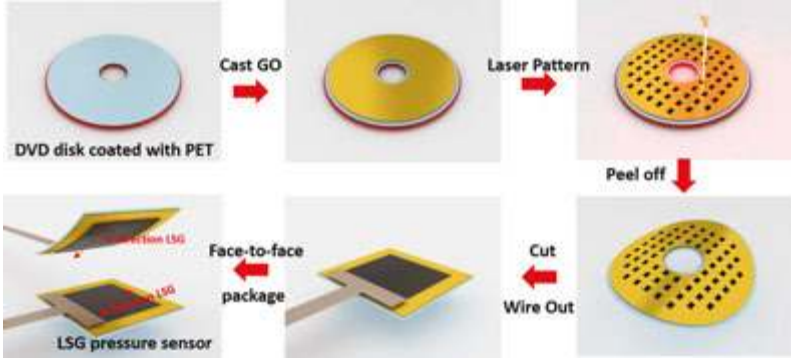

Figure 19. Fabrication process for the LSG pressure sensor. Reprinted from Ref. [14] (CC BY 4.0).

The working principle of the LSG pressure sensor can be described as follows (**Figure 20**): when a force is applied on top, the inter layer distance of the LSG is reduced, which can change the resistance of the LSG. Since LSG has a porous structure, the force can not only increase the contact area but also increase the density of the LSG. Both these effects can increase the current

http://dx.doi.org/10.5772/64228

pathway. When the pressure is released, the LSG foam releases and the interlayer distance recovers, which can lower the current to its initial level.

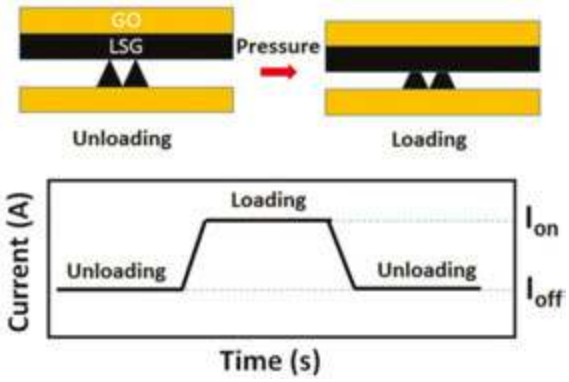

Figure 20. The working principle of the LSG pressure sensor. Reprinted from Ref. [14] (CC BY 4.0).

In order to test the LSG pressure sensor, we have set up a force testing system. This system contains a motor, a pressure sensor and a resistance analyser. In this system, a static force up to 113 kPa can be applied and the resistance analyser can acquire the resistance from the LSG pressure sensor simultaneously. As shown in **Figure 21**, if the pressure sensing range is up to 50 kPa, the sensitivity can be as high as 0.96 kPa^{-1}. This indicates that the contact area and density obviously change in this pressure range. When the pressure is larger than 50 kPa, the pressure sensor starts to saturate with a sensitivity of 0.005 kPa^{-1}. This demonstrates that we have successfully obtained a high sensitivity pressure sensor using laser-scribing technology.

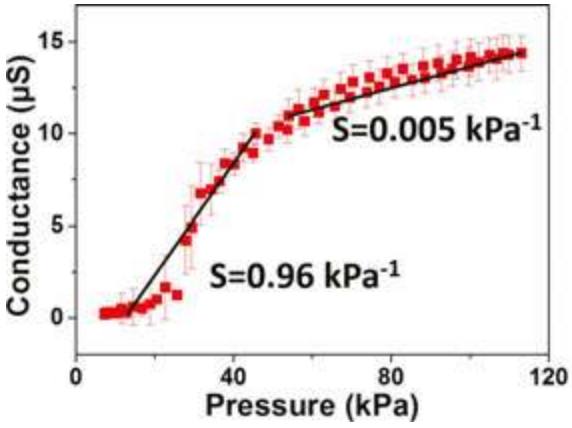

Figure 21. Testing results of the LSG pressure sensor. Reprinted from Ref. [14] (CC BY 4.0).

3.5. Graphene light-emitting device

In conventional light-emitting devices, the emission wavelength cannot be changed after the devices are fabricated. This is because the bandgap of the material cannot be modified. Previously, there was no report on light-emitting devices with tunable wavelength in a wide range. Here, we obtained a wavelength tunable graphene light-emitting device based on laser-scribing technology [15].

Figure 22. Device structure of the graphene light-emitting device. The semi-rGO layer functions as the light-emitting layer. Reprinted from Ref. [15] (CC BY 4.0).

As shown in **Figure 22**, a graphene in-plane transistor can be fabricated, based on laser-scribing technology. An in-plane transistor means that the gate, source and drain are all in the same plane. The gate electrical field can be applied to channel through the in-plane GO dielectric. All the components, namely the channel, source, drain and gate can be fabricated in a single laser-scribing step. After the device fabrication, a large current is applied to the channel (mA), which can burn the upper rGO away and expose the interface layer consisting of semi-rGO. A striking feature is that the whole fabrication process does not need vacuum or high temperature.

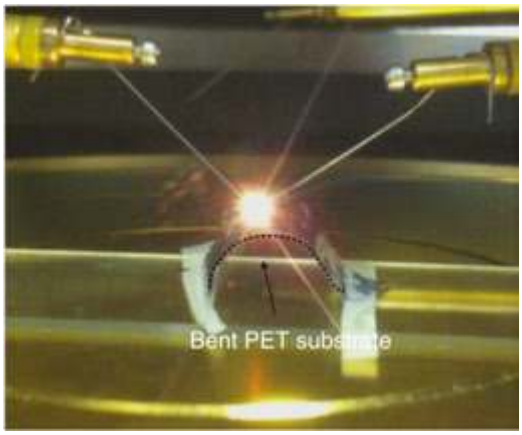

Figure 23. Flexible graphene light-emitting device with red light emission. Reprinted from Ref. [15] (CC BY 4.0).

http://dx.doi.org/10.5772/64228

When the device is driven by a voltage of 10 V, there is a noticeable red light emission (**Figure 23**). Moreover, as it is directly fabricated on a PET substrate, the whole device is flexible. **Figure 24** shows the light emission spectra under different gate voltages. Each curve shows a single Lorentzian shape. When the gate voltage is zero, the light wavelength is around 690 nm. When the gate voltage is 50 V, the wavelength shifts to 470 nm. This indicates that increasing the gate voltage can shift the wavelength to a lower value. Moreover, the blue light emission efficiency is much lower than the red light efficiency from the intensity shown in the spectrum. Under different gate voltages, the selected semi-rGO is excited to emit light. The light emission mechanism can be explained by the Poole–Frenkel effect. Under a strong electrical field, the electrons can be excited by impact ionization effect and recombined with the holes. The extra energy can be released by emission of photons.

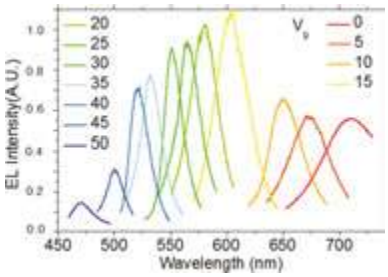

Figure 24. Different light emission spectra, obtained by tuning the gate voltage. Reprinted from Ref. [15] (CC BY 4.0).

3.6. Wafer-scale graphene devices integration

Since a variety of graphene devices can be easily patterned onto the GO film via the laser-scribing technology, it is possible to integrate multifunctional graphene devices [16] over an entire wafer (**Figure 25**). As shown in **Figure 25a**, a graphene transistor, photodetector and loudspeaker were integrated on the same chip. Furthermore, the substrates could even be flexible (**Figure 25b**). The patterning process of a whole wafer was finished in 25 min. This development brings our field one-step closer to the concept of heterogeneous integration, and it would be useful to investigate this technique and platform in further detail.

Figure 25. Wafer-scale graphene devices integration. (a) Multifunctional graphene devices containing transistors, photodetectors and loudspeakers. (b) Flexible graphene devices. (c) Wafer-scale graphene devices. Reprinted by permission from Macmillan Publishers Ltd: Scientific Reports (4:3598), copyright (2014) [16].

4. Outlook: ion scribing for graphene oxide reduction

The outstanding success of laser scribing for rGO-based device fabrication naturally leads one to imagine whether other serial writing techniques can be used as well. Besides laser lithography, other serial writing techniques include electron beam lithography, ion beam lithography, proton beam lithography and X-ray (or synchrotron) lithography. A review of literature reveals that reduction of GO has already been briefly investigated with electron beam lithography [17] and ion beam lithography [18]. Although the conversion efficiency of electron beam lithography for graphene oxide reduction is very low, and hence impractical, ion beam lithography is very promising. Lobo et al. [18] have investigated the morphology, composition and conductivity changes and confirmed the reduction of GO by Gallium ions. We have also begun investigations using ion beam lithography for GO reduction and device fabrication, and we observed that the conductivity of 300 nm GO films on SiO_2/Si conducts up to 1.8×10^{-10} A (0.18 pA) for a Ga^+ ion dose of 750 μC/cm^2, as shown in **Figure 26** [19].

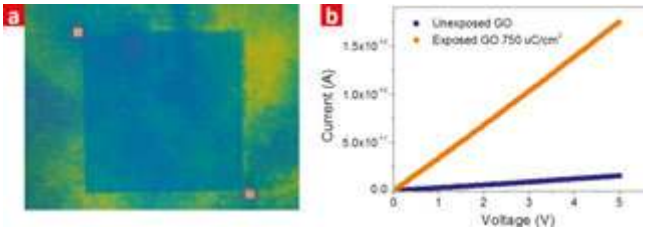

Figure 26. GO reduction by Ga^+ ion beams showing (a) the exposed and unexposed areas, and (b) the increase in conductivity at a dose of 750 μC/cm^2, as compared with unexposed GO.

5. Summary

In this chapter, the fabrication of wafer-scale graphene devices by one-step laser-scribing technology is demonstrated. Five kinds of novel graphene devices were developed, including a memory, an earphone, a strain sensor, a pressure sensor and a light-emitting device. The graphene resistive memory has a Fin-like structure with forming-free behaviour, stable switching, reasonable reliability and potential for 2-bit storage. The graphene earphone enables wide-band sound generation from 100 Hz to 50 kHz, which can be used for both humans and animals. The strain sensor based on graphene micro-ribbons has a gauge factor up to 9.49. The sensitivity of the graphene pressure sensor is as high as 0.96 kPa^{-1} in a wide pressure range (0∼50 kPa). A graphene light-emitting device is also developed with a tuneable emission wavelength. These results demonstrate that laser-scribing technology can be used as a platform to develop novel graphene devices. As a serial lithography technique, at the forefront of controlled graphene oxide reduction, laser scribing serves as a model for similar developments in other patterning techniques, such as ion beam lithography.

Author details

He Tian[1,2], Mohammad Ali Mohammad[1,3], Wen-Tian Mi[1], Yi Yang[1] and Tian-Ling Ren[1*]

*Address all correspondence to: RenTL@tsinghua.edu.cn

1 Institute of Microelectronics and Tsinghua National Laboratory for Information Science and Technology (TNList), Tsinghua University, Beijing, China

2 Ming Hsieh Department of Electrical Engineering, University of Southern California, Los Angeles, CA, United States

3 School of Chemical and Materials Engineering (SCME), National University of Sciences and Technology (NUST), Sector H-12, Islamabad, Pakistan

References

[1] Geim AK, Novoselov KS. The rise of graphene. Nature Materials. 2007;6:183-191. DOI: 10.1038/nmat1849

[2] Bolotin KI, Sikes KJ, Jiang Z, Klima M, Fudenberg G, Hone J, Kim P, Stormer HL. Ultrahigh electron mobility in suspended graphene. Solid State Communications. 2008;146(9):351-355. DOI:10.1016/j.ssc.2008.02.024

[3] Mak KF, Ju L, Wang F, Heinz TF. Optical spectroscopy of graphene: From the far infrared to the ultraviolet. Solid State Communications. 2012;152(15):1341–1349. DOI: 10.1016/j.ssc.2012.04.064

[4] Lee C, Wei X, Kysar JW, Hone J.. Measurement of the elastic properties and intrinsic strength of monolayer graphene. Science. 2008;321(5887):385-388. DOI: 10.1126/science. 1157996

[5] Balandin AA, Ghosh S, Bao W, Calizo I, Teweldebrhan D, Miao F, Lau CN. Superior thermal conductivity of single-layer graphene. Nano Letters. 2008;8(3):902-907. DOI: 10.1021/nl0731872

[6] Hummers Jr, WS., Offeman RE. Preparation of graphitic oxide. Journal of the American Chemical Society. 1958;80(6):1339. DOI: 10.1021/ja01539a017

[7] Dreyer DR, Park S, Bielawski CW, Ruoff RS. The chemistry of graphene oxide. Chemical Society Reviews. 2010;39(1):228-240. DOI: 10.1039/B917103G

[8] Eda G, Fanchini G, Chhowalla M. Large-area ultrathin films of reduced graphene oxide as a transparent and flexible electronic material. Nature Nanotechnology. 2008;3(5): 270-274. DOI: 10.1038/nnano.2008.83

[9] El-Kady MF, Strong V, Dubin S, Kaner RB. Laser scribing of high-performance and flexible graphene-based electrochemical capacitors. Science. 2012;335(6074):1326-1330. DOI: 10.1126/science.1216744

[10] El-Kady MF, Kaner RB. Scalable fabrication of high-power graphene micro-super capacitors for flexible and on-chip energy storage. Nature Communications. 2013;12(4): 1475. DOI: 10.1038/ncomms2446

[11] Tian H, Chen HY, Ren TL, Li C, Xue QT, Mohammad MA, Wu C, Yang Y, Wong HS. Cost-effective, transfer-free, flexible resistive random access memory using laser-scribed reduced graphene oxide patterning technology. Nano Letters. 2014;14(6):3214–3219. DOI: 10.1021/nl5005916

[12] Tian H, Li C, Mohammad MA, Cui YL, Mi WT, Yang Y, Xie D, Ren TL. Graphene earphones: entertainment for both humans and animals. ACS Nano. 2014;8(6): 5883-5890. DOI: 10.1021/nn5009353

[13] Tian H, Shu Y, Cui YL, Mi WT, Yang Y, Xie D, Ren TL. Scalable fabrication of high-performance and flexible graphene strain sensors. Nanoscale. 2014;6(2):699-705. DOI: 10.1039/C3NR04521H

[14] Tian H, Shu Y, Wang XF, Mohammad MA, Bie Z, Xie QY, Li C, Mi WT, Yang Y, Ren TL. A graphene-based resistive pressure sensor with record-high sensitivity in a wide pressure range. Scientific Reports. 2015;5:8603. DOI: 10.1038/srep08603

[15] Wang X, Tian H, Mohammad MA, Li C, Wu C, Yang Y, Ren TL. A spectrally tunable all-graphene-based flexible field-effect light-emitting device. Nature Communications. 2015;6:7767. DOI: 10.1038/ncomms8767

[16] Tian H, Yang Y, Xie D, Cui YL, Mi WT, Zhang Y, Ren TL. Wafer-scale integration of graphene-based electronic, optoelectronic and electroacoustic devices. Scientific Reports. 2014;4:3598. DOI: 10.1038/srep03598

[17] Chen L, Xu Z, Li J, Min C, Liu L, Song X, Chen G, Meng X. Reduction and disorder in graphene oxide induced by electron-beam irradiation, Materials Letters. 2011;65:1229. DOI: 10.1016/j.matlet.2011.01.063

[18] Lobo DE, Fu J, Gengenbach T, Majumder M. Localized deoxygenation and direct patterning of graphene oxide films by focused ion beams. Langmuir. 2012;28:14815. DOI: 10.1021/la303369m

[19] Mohammad MA, Mi WT, Li YX, Tian H, Yang Y, Ren TL. Manuscript in preparation (2016).